IEEE Access
Multidisciplinary | Rapid Review | Open Access Journal

Received 17 January 2024, accepted 13 February 2024, date of publication 21 February 2024, date of current version 4 March 2024.

Digital Object Identifier 10.1109/ACCESS.2024.3368804

RESEARCH ARTICLE

Block Scalable OFDM-Based Waveform for NTN Uplink–A Comparative Study of Multiple Candidate Waveforms Over NTN Scenarios Using NR Numerology

YUFAN CHEN[1], HAN LIU[1], ZHIPING LU[2,3], AND HUA WANG[1], (Member, IEEE)
[1]School of Information and Electronics, Beijing Institute of Technology, Beijing 100081, China
[2]School of Information and Communication Engineering, Beijing University of Posts and Telecommunications, Beijing 100876, China
[3]State Key Laboratory of Wireless Mobile Communications, China Academy of Telecommunications Technology (CATT), Beijing 100191, China

Corresponding authors: Han Liu (liuhan4335@bit.edu.cn) and Hua Wang (wanghua@bit.edu.cn)

This work was supported in part by the National Key Research and Development Program of China under Grant 2020YFB1807900; in part by the State Key Laboratory of Wireless Mobile Communications, China Academy of Telecommunications Technology (CATT); in part by the National Natural Science Foundation of China under Grant 62205028; and in part by Datang Linktester Technology Company Ltd.

ABSTRACT Non terrestrial network (NTN) has been regarded as an important component of beyond 5G communication. The 3rd Generation Partnership Project (3GPP) has officially started studies on NTN for the purpose of integrating satellites with New Radio (NR) terrestrial networks. However, the NR defined orthogonal frequency division multiplexing (OFDM) waveform is susceptible to doubly selective fading and nonlinear distortions in the NTN uplink, thus leading to severe performance loss. In this paper, a type of block scalable OFDM (BS-OFDM) waveform is proposed, which has modified subcarrier and sub-symbol segmentation when compared to the conventional NR defined OFDM. With our proposed framework, block scalable discrete Fourier transform spread OFDM (BS-DFT-s-OFDM) and block scalable orthogonal time frequency space (BS-OTFS) can also be implemented. To obtain a comprehensive understanding of different waveforms, performance metrics concerning peak to average power ratio (PAPR), total degradation (TD), bit error rate (BER), and complexity are presented. The simulation results demonstrate that the proposed block scalable waveforms can obtain better performance and lower complexity than existing NR waveforms in different NTN uplink scenarios, and can therefore be promising candidate waveforms for NR NTN.

INDEX TERMS Block scalable OFDM, DFT-s-OFDM, doubly selective fading, nonlinear HPA, NR protocol, NTN uplink, OTFS.

I. INTRODUCTION

A non terrestrial network (NTN) refers to a network or segment of networks using radio frequency resources on board a satellite or unmanned aircraft system (UAS) platform [1]. NTN can provide ubiquitous coverage and reduce the vulnerability of space/airborne vehicles to physical attacks and natural disasters, which has attracted the attention of both industry and academia [2]. Accordingly, the 3rd Generation Partnership Project (3GPP) has officially started studies on NTN for the purpose of integrating satellites with 5G New Radio (NR) terrestrial networks, where the deployments of orthogonal frequency division multiplexing (OFDM) based air interfaces over satellite links were suggested by the 3GPP NTN activities [3]. However, OFDM is susceptible to high Doppler shift, which causes intercarrier interference and eventually results in severe performance degradation [4]. The Doppler shift depends on the relative speed of the space/airborne platforms, the speed of the user equipment, and the carrier frequency. Therefore, the NTN channel may experience higher Doppler shifts than traditional terrestrial systems due to the higher mobility of non-stationary satellites

The associate editor coordinating the review of this manuscript and approving it for publication was Mohamed M. A. Moustafa.

or user equipment [5], [6]. Further, multiple Doppler shift of multipath is difficult to be pre-compensated, especially for low-cost user equipment [7]. Moreover, the nonlinear characteristic of high power amplifier (HPA) is also non-negligible in NTN uplink. The performance of NR defined OFDM with traditional frequency domain equalization (FDE) degrades significantly, since high Doppler shift destroys the orthogonality between subcarriers. The high peak to average power ratio (PAPR) of NR defined OFDM also makes it sensitive to nonlinear distortions [8].

A. RELATED WORKS

To enable efficient and reliable transmission, the performance of single-carrier and multi-carrier waveforms over satellite links has been extensively studied. In [9], single-carrier frequency division multiple access (SC-FDMA) has been studied in the return link of satellite networks, which showed that SC-FDMA allows decreasing receiver complexity for comparable spectral and power efficiency performance with single-carrier time division multiple access (SC-TDMA). In [10], the performance of orthogonal frequency division multiple access (OFDMA), localized FDMA (LFDMA), and interleaved FDMA (IFDMA) were compared under flat fading channel considering nonlinear distortion and asynchronous inter block interference (IBI), which showed that LFDMA outperformed the other two waveforms under asynchronous scenarios. The authors of [11] investigated the performances of OFDM and minimum frequency shift keying (MSK) modulations as potential global navigation satellite systems (GNSS) signal modulation schemes, the results showed that OFDM demonstrated promises as a viable GNSS modulation with larger bandwidths. The performance assessment of 5G NR physical layer aspects for satellite applications was carried out in [12], which showed that OFDM can fulfill the communication requirements in scenarios with flat fading and low receiver speed. In [13] and [14], filtered-OFDM, windowed-OFDM, and their discrete Fourier transform (DFT) spread counterparts were considered to mitigate out of band emissions (OOBE), where filtered-OFDM is recommended as a promising candidate for the satellite to user link. In [15], OFDM and DFT spread OFDM (DFT-s-OFDM) were compared with digital video broadcasting-satellite-second generation extension (DVB-S2X) defined single-carrier waveform with root raised cosine (RRC) pulse under NTN downlink with nonlinear HPA, which showed that OFDM faces significant performance degradation under nonlinear power amplifier, and an SC waveform option in the downlink can be beneficial. Some other works focused on multicarrier waveform or transmission scheme design in satellite communication systems [16], [17], [18]. The authors of [16] studied the application of coded OFDM for broadband satellite transmission in the forward link, where successive correction techniques were proposed to compensate for the nonlinear distortions. The authors of [17] proposed a pre-distortion-based index-modulated OFDM (IM-OFDM) for the terrestrial-satellite radio link and showed that it can achieve a better tradeoff among BER performance and HPA efficiency when compared with OFDM and IM-OFDM systems. A recent work proposed an OFDM with binary offset carrier (OFDM-BOC) for GNSS [18], the authors demonstrated that OFDM-BOC has better navigation performance and lower complexity than OFDM through both simulations and analysis. However, only small Doppler shifts were considered in the above mentioned studies, which were not suitable for high mobility NTN uplink scenarios.

In addition, promising waveforms such as orthogonal time frequency space (OTFS) also draw significant attention. Specifically, OTFS is proposed for high mobility communications, which modulates the symbols in the delay Doppler (DD) domain. As a result, all symbols experience the same channel gain in both the time and the frequency domain, which enables full diversity to be realized with proper channel equalization [19]. The channel equalization is more practical and robust thanks to the sparsity and lower variability of the DD domain channel [20]. Some existing works focused on OTFS based waveform design to optimize the modulation methods at the transmitter to improve the system performance [21], [22], [23], [24], [25]. Modulation schemes like index modulation are also applicable to OTFS to further improve spectrum efficiency, diversity, and PAPR performance [21], [22]. The authors of [23] and [24] combined spatial modulation and generalized spatial modulation with the multiple input multiple output OTFS (MIMO-OTFS) system to improve spectral efficiency and BER performance. In [25], the authors proposed a 3D-OTFS modulation to improve the BER performance under high modulation orders. Some other studies focused on the performance comparison of OTFS with other waveforms under different channel conditions [26], [27], [28], [29], where the superiority of OTFS over other candidate waveforms in terms of diversity was highlighted, which made OTFS more attractive in high mobility communication systems.

Recently, a few studies have investigated the potential of OTFS over satellite links. In [30], [31], and [32], the authors investigated the secrecy and reliability performance of OTFS-based low earth orbit (LEO) satellite communication systems, where the closed-form outage probability was derived, showing the superiority of OTFS compared to OFDM. In [33], the performance of OTFS under LEO downlink channel was studied, where OTFS is observed to be robust across various channel models. In [34], the authors proposed a dual satellite transmission scheme using precoded OTFS to improve spectral efficiency and link reliability. In [35], a blind separation scheme was proposed using the sparsity of the DD domain signal. In [36], the authors proposed an OTFS modulation for reconfigurable intelligent surface (RIS) aided space–air–ground integrated networks. In [37], a joint channel estimation and data detection algorithm for OTFS systems based on variational Bayesian inference (VBI) was proposed. In [38], [39], [40], [41], and [42], OTFS was

TABLE 1. Contrasting our contributions to the literature.

Feature	[9], [10]	[12]– [15]	[16]	[17]	[18]	[21]– [25], [30]– [32], [34], [36]	[26]– [29], [33]	This paper
Novel waveforms/ transmission schemes			✓	✓	✓	✓		✓
Compatibility with NR frame structure	✓	✓	✓					✓
Symbol re-segmentation								✓
Multipath fading		✓		✓	✓	✓	✓	✓
High Doppler shifts						✓	✓	✓
Nonlinear distortions of HPA	✓	✓	✓	✓				✓
Fair comparison under NTN deployments								✓

integrated with grant-free multiple access to support massive user access in LEO satellite scenarios.

The above studies on OTFS mainly focused on transmission schemes design for performance improvement, however lack consideration for compatibility with the existing NR protocol [43]. Due to significant modifications to the frame structure of OTFS with respect to OFDM, the protocol defined procedures need to be redesigned when integrated with NR. Further, the nonlinearity of HPA has not been studied in these works. It is worth noting that the PAPR of OTFS grows with the symbol number [44], [45]. On the other hand, the variations of subcarrier number and symbol number also affect the diversity gain and complexity greatly. Coexisting with NR, as well as trading-off among diversity, PAPR, and complexity, are vital problems to be solved for waveform design in NTN uplink.

B. CONTRIBUTIONS

In contrast to OTFS that modifies the total frequency and time occupancy of the NR resource grid, in this paper we maintain the total frequency and time occupancy, while the subcarrier and sub-symbol number of the NR resource grid are modified. A new waveform called block scalable OFDM (BS-OFDM), which is compatible with other existing NR procedures, is proposed in this paper. The proposed waveform shows better flexibility in diversity, lower PAPR, and lower complexity, and is also compatible with DFT spread and OTFS pre-processings. Block equalization (BE) is uniformly utilized at the receiver, which outperforms FDE since channel variation is taken into consideration. To verify the superiority of the proposed waveforms, performance comparisons of BS waveforms with existing NR waveforms under different nonlinear NTN uplink scenarios are provided. The novel contributions of this paper contrasting to the literature are listed in Table 1.

The main contributions of this paper are summarized as follows:

1) BS-OFDM based waveform is proposed. The proposed waveform can maintain the same time and frequency occupancy with OFDM, and can be extended to DFT spread and OTFS counterparts with improved performance in NTN uplink.

2) Qualitative evaluations on diversity and PAPR, as well as quantitative complexity analysis, are provided, which demonstrate that BS-OFDM can achieve higher flexibility in diversity selection, lower PAPR, and lower complexity than existing OFDM waveform at the same data rate. These actions present a perspective for further recognizing the potential benefits of applying BS-OFDM in NTN uplink, and fill the gaps of existing works on waveforms in the capabilities of trading off among diversity, PAPR, and complexity.

3) Comparison schemes under NTN scenarios are provided according to 3GPP NR protocol and NTN deployments. The PAPR, total degradation (TD), nonlinear BER, and complexity results of different waveforms under NTN scenarios are provided.

The rest of this paper is organized as follows, Section II introduces the channel fading model and HPA nonlinear characteristics of NTN. Section III first provides an overview of NR defined OFDM and OTFS, then introduces the proposed BS-OFDM based waveform. In Section IV, the performances of different candidate waveforms under the NTN channels are simulated and compared. In Section V, we conclude this paper. In Section VI, we point out some topics of future work.

Notations: The superscripts $(.)^T$, $(.)^*$, $(.)^H$ and $(.)^n$ represent the transpose, conjugate, conjugate transpose, and nth-power operation, respectively. $|.|$ is the absolute value, $E(.)$ is the expectation operator, and $\sum(.)$ is the summation operator. The notation $*$ denotes the convolutional product. The normalized N-point DFT and IDFT matrices are denoted by $\mathbf{F}_N$ and $\mathbf{F}_N^H$, respectively.

II. NTN CHANNEL CHARACTERISTICS

A. CHANNEL MODEL

The NTN channel is modeled concerning the presence of obstacles, relative movements of both the NTN platform and the user equipment (UE), NTN platform altitude and orbit, and frequency bands, etc. [46]. For NTN propagation channel modeling, both multipath fading and Doppler shift are considered. The following frequency bands will be in particularly considered (For very small aperture terminal (VSAT), Ka band, Uplink: 29.5 – 30.0 GHz; For handheld user equipment, S band, Uplink: 1980 - 2010 MHz.) [2].

For link level modeling of multipath delay, two types of channel models, namely clustered delay line (CDL) and tapped delay line (TDL), are suggested [2]. CDL models can be used to depict S and Ka bands, which are applicable to different environments and elevation angles. TDL models are

used for single input single output (SISO) evaluations, which can be filtered from CDL models by assuming isotropic UE antenna at transmitter and receiver.

Considering an NTN uplink channel with P paths. The Doppler shift of the i th path is a summation of the Doppler shift caused by the motion of the satellite and the UE, which can be expressed as

$$f_{d,i} = f_{d,SAT,i} + f_{d,UE,i}. \quad \forall i = 1, \ldots, P \tag{1}$$

where the Doppler shift caused by the motion of UE is given by

$$f_{d,UE,i} = v_{UE} \times \cos(\theta_i) \times \frac{f_c}{c}, \tag{2}$$

where v_{UE}, c and f_c are the velocity of the UE, the velocity of light and carrier frequency, respectively, θ_i is the angle between the UE moving direction and the direction of i th path from the UE. It is further assumed that the UE moves in all directions with the same probability and that the scatterers are located uniformly around the UE. Thus θ_i is assumed to be uniformly distributed between $[-\pi, \pi]$ and independent for each path.

For non-geostationary earth orbit (non-GEO) satellites, additional Doppler shift caused by satellite motion should be taken into account, which is given by

$$f_{d,SAT,i} = v_{SAT} \times \cos(\psi_i) \times \frac{f_c}{c}, \tag{3}$$

where v_{SAT} is the velocity of the satellite, ψ_i is the angle between the satellite moving direction and the direction of i th path from the satellite.

Typically, ψ_i is uniformly distributed between $[0, \pi]$. Since the distance between the satellite and UE is much longer than the scatterers, the difference in ψ_i for different paths can be neglected.

B. NONLINEAR CHARACTERISTICS OF HPA

In NTN payload architecture, in order to compensate for large propagation loss, high power amplifier is a crucial component. However, the nonlinearity of HPA becomes obvious when it works near the saturation region, which leads to constellation warping and clustering, thus deteriorating the system performance [2].

To depict the HPA nonlinearity, a simplified memoryless modified Saleh Model can be used to model its amplitude-to-amplitude (AM/AM) characteristics [49]. Fig.1 illustrates the AM/AM characteristics of the HPA. We assume that the saturation amplitude of HPA is $SA = 0$dB.

The output of HPA corresponding to input $u = ae^{j\arg(u)}$ can be expressed as

$$z = T(a)e^{j(\arg(u)+\phi(a))}, \tag{4}$$

where $T(a)$ and $\phi(a)$ are the AM/AM and amplitude-to-phase (AM/PM) functions of the HPA, respectively. In fact, the phase distortion $\phi(a)$ caused by the HPA can be pre-calculated and subtracted from the original signal before input to the HPA, which can be assumed to be perfectly corrected. The amplitude distortion in the nonlinear region of HPA can be corrected using a predistortion method which ensures that $T(T^{-1}(a)) = a$. However, the clipping caused by HPA saturation cannot be corrected through predistortion operations. For simplicity and without loss of generality, the cascaded combination of a predistorter and the HPA can be simplified as a soft envelope limiter [50], [51], the output z_{pd} corresponding to the input $u = ae^{j\arg(u)}$ is expressed as

$$z_{pd} = \begin{cases} u, & a \le SA \\ SAe^{j\arg(u)}, & a > SA \end{cases}. \tag{5}$$

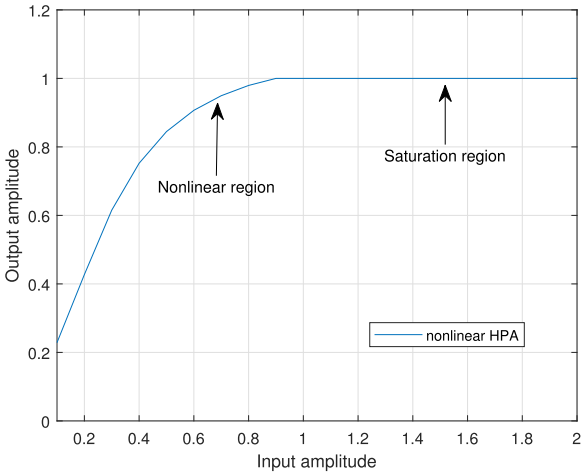

FIGURE 1. AM/AM characteristics of HPA.

III. BLOCK SCALABLE OFDM BASED NTN WAVEFORM DESIGN

A. NR PROTOCOL DEFINED OFDM & DFT-s-OFDM

In NR protocol, orthogonal frequency division multiplexing (OFDM) is the commonly adopted waveform, which modulates the signal onto multiple orthogonal subcarriers for efficient and robust transmission. The time frequency resource structure of NR defined OFDM is shown in Fig.2. In OFDM, the data symbols generated by constellation mapping are modulated onto a number of OFDM symbols with M orthogonal subcarriers. The data subcarriers in one OFDM symbol can be denoted in vector form as $\mathbf{X} \in \mathbb{C}^{M\times 1}$. The M subcarriers are zero padded into $Nfft$ contiguous subcarriers in the frequency domain, then the subcarriers are transformed into the time domain OFDM symbol through an inverse discrete Fourier transform (IDFT) operation, given by

$$\mathbf{x} = \mathbf{F}_{Nfft}^H \mathbf{Z}\mathbf{X}, \tag{6}$$

where $\mathbf{Z} \in \mathbb{C}^{Nfft\times M}$ is a zero padding matrix, $\mathbf{F}_{Nfft}^H$ is the normalized $Nfft$ -point IDFT matrix. The frequency domain (FD) zero padding and IDFT operations are equivalent to upsampling and filtering using a perfect rectangular pulse. For the l th symbol in a slot, a cyclic prefix (CP) with $N_{CP,l}^{sample}$ samples is added to avoid inter-symbol interference (ISI) and

guarantee the cyclic convolution. Accordingly, the reception process can be expressed as

$$\mathbf{Y}_{RCP} = \mathbf{F}_{Nfft}\mathbf{y}_{RCP} = \mathbf{F}_{Nfft}\mathbf{x} \cdot \mathbf{F}_{Nfft}\mathbf{h} + \mathbf{F}_{Nfft}\mathbf{n}_{RCP}, \quad (7)$$

where $\mathbf{y}_{RCP} \in \mathbb{C}^{Nfft}$ and $\mathbf{n}_{RCP} \in \mathbb{C}^{Nfft}$ are the received signal and noise vector after CP removal, respectively, $\mathbf{h} \in \mathbb{C}^{L\times 1}$ is the channel impulse response (CIR) with a maximum multipath delay of $L-1$ samples. To compensate for the frequency selective fading caused by multipath, frequency domain equalization (FDE) can be implemented. Benefiting from the simplicity of a point-wise equalizer in the discrete frequency domain, FDE is the most general channel equalization method in OFDM [52]. The FDE implementation is given by

$$\mathbf{Y}_{eq} = \mathbf{C} \cdot \mathbf{Y}_{RCP}, \quad (8)$$

where $\mathbf{Y}_{eq} \in \mathbb{C}^{Nfft\times 1}$ is the equalized OFDM symbol and $\mathbf{C} \in \mathbb{C}^{Nfft\times 1}$ is the FD point-wise equalizer. Typically, the coefficients of zero forcing (ZF) equalizer can be expressed as

$$\mathbf{C}(k) = 1/\mathbf{H}(k), \quad (9)$$

and the coefficients of minimum mean square error (MMSE) equalizer can be expressed as

$$\mathbf{C}(k) = \mathbf{H}^*(k)/\left(\mathbf{H}^*(k)\mathbf{H}(k) + \sigma^2\right), \quad (10)$$

where $\mathbf{H} = \mathbf{F}_{Nfft}\mathbf{h}$ is the channel frequency response (CFR), $\mathbf{C}(k)$ and $\mathbf{H}(k)$ are the equalizer and CFR coefficients of the k th subcarrier, respectively, and σ^2 is the noise variance.

NR protocol introduces the multiple OFDM numerologies that specify subcarrier spacing (SCS), CP length, slot number, etc. [43]. The scalable numerologies enable network flexibility and scalability in supporting different applications [53]. To be specific, the subcarrier spacing Δf has an exponential relation with the SCS configuration μ, given by

$$\Delta f = 2^{\mu} \times 15\,[kHz]. \quad (11)$$

The system bandwidth and sample rate are $BW = M\Delta f$ and $SR = Nfft\Delta f$, respectively. The CP time length for extended CP (ECP) and normal CP (NCP) have negative exponential relations with μ as follows

$$N^{\mu}_{\mathrm{CP},l} = \begin{cases} 512\kappa \cdot 2^{-\mu} & \text{ECP} \\ 144\kappa \cdot 2^{-\mu} + 16\kappa & \text{NCP, } l = 0 \text{ or } l = 7\cdot 2^{\mu} \\ 144\kappa \cdot 2^{-\mu} & \text{NCP, } l \neq 0 \text{ and } l \neq 7\cdot 2^{\mu}, \end{cases} \quad (12)$$

where $\kappa = T_s/T_c$ is a constant, T_s is the duration of time sample with a reference bandwidth of 2048 × 15kHz and T_c is the basic time unit of NR, l is the symbol number in the subframe. Generally, the parallel data stream number M is chosen to be a multiple of N^{RB}_{SC}, which is the subcarrier number in a resource block and equals to 12. The IDFT size $Nfft$ follows three rules: 1) The size is a power of 2. 2) Maximum occupancy $M/Nfft \leq 85\%$. 3) $Nfft \geq 128$ so that

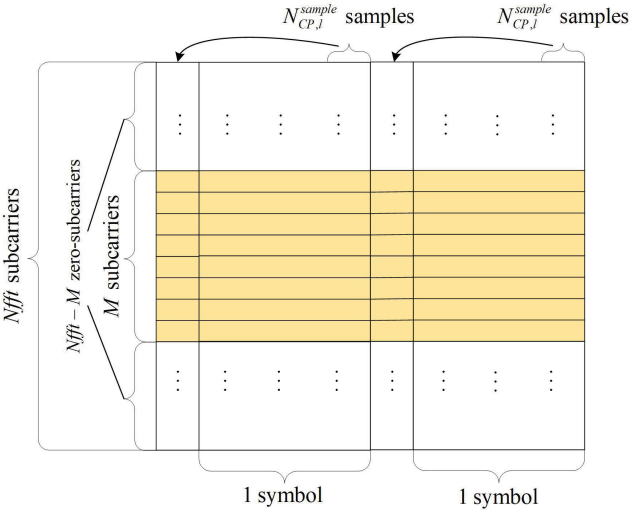

FIGURE 2. Time frequency structure of NR defined OFDM.

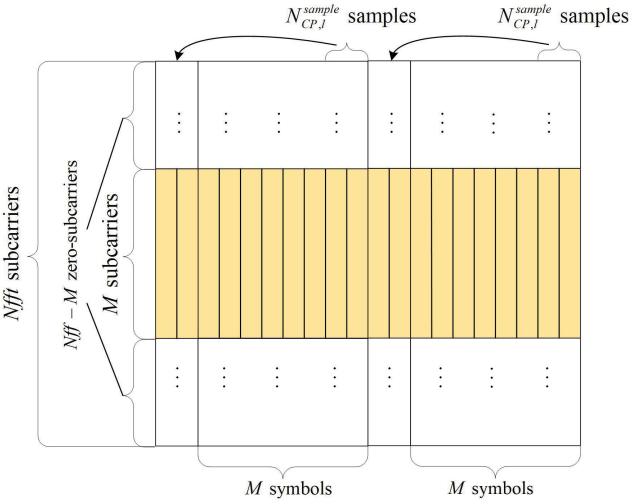

FIGURE 3. Time frequency structure of NR defined DFT-s-OFDM.

the cyclic prefix sample length $N^{sample}_{CP,l} = N^{\mu}_{\mathrm{CP},l} \times SR \times T_c$ is always an integer.

Unfortunately, in high mobility NTN channels, the high Doppler effect leads to intercarrier interference (ICI) and severely destroys the orthogonality of subcarriers [4], [36], which cannot be easily handled, especially for NTN uplink equipment. Although the SCS of the OFDM signal may be extended with greater values to accommodate larger Doppler shift, this will bring new problems. Specifically, by substituting (11) into (12) and eliminating μ, it can be observed that the CP time length $N_{\mathrm{CP},l}$ is inversely proportional to subcarrier spacing Δf. This means direct increment of SCS will shorten the time length of CP, which may cause severe inter symbol interference (ISI) in some NTN channels where the maximum delay is larger than the CP time length.

Other demerits of NR defined OFDM include high PAPR and low frequency diversity order, which lead to higher sensitivity to nonlinear distortion and frequency domain deep fading [8].

DFT-s-OFDM is the DFT precoded form of OFDM. The time frequency structure is shown in Fig.3. DFT-s-OFDM applies an M point DFT spread before zero padding, which can be presented as

$$\mathbf{x} = \mathbf{F}_{Nfft}^{H}\mathbf{Z}\mathbf{F}_{M}\mathbf{X}. \tag{13}$$

The entire operation is equivalent to cyclically convolving the data symbols with the Dirichlet sinc function in the time domain, which retains single-carrier benefits. Then, similar operations as OFDM, including CP insertion, CP removal, and channel equalization, can be used to handle the signal. The superiority of DFT-s-OFDM over other single-carrier and multi-carrier waveforms has been demonstrated in [54]. Due to its low PAPR and excellent efficiency in frequency division multiple access, DFT-s-OFDM is employed as a candidate waveform for long term evolution (LTE) and NR uplinks. Nevertheless, it comes at the cost of increased complexity and reduced time diversity order.

B. FUNDAMENTAL OF OTFS

Orthogonal time frequency space (OTFS) has been proposed as a promising candidate waveform for high mobility communications, owing to its advantages in handling the problems caused by the Doppler effect [19]. Unlike other waveforms that perform data modulation in the time-frequency (TF) domain, OTFS modulates data in the DD domain, thereby converting the time-varying channel in the TF domain into a quasi-time-invariant channel in the DD domain, which in turn ensures that the transmission frame symbols experience almost constant channel gain [20]. Therefore, OTFS can be regarded as an ideal solution for high-Doppler multipath channels. Additionally, OTFS can fully utilize the diversity of time-varying frequency selective channels and offer significant delay and Doppler resilience, which makes OTFS more competitive in high mobility communication systems [47].

As shown in Fig.4, the data symbols are mapped into the DD domain block $\mathbf{X}_{OTFS} \in \mathbb{C}^{M\times N}$ with M delay bins and N Doppler bins. The TF domain block is obtained through an inverse symplectic finite Fourier transform (ISFFT), which is equivalent to an M-point DFT and an N-point IDFT of the columns and rows of $\mathbf{X}_{OTFS}$, given by

$$\mathbf{X} = \mathbf{F}_{M}\mathbf{X}_{OTFS}\mathbf{F}_{N}^{H}, \tag{14}$$

where the TF block $\mathbf{X} = [\mathbf{X}_1, \mathbf{X}_2, \ldots, \mathbf{X}_N]$ is a concatenation of N OFDM symbols with M subcarriers. The time domain waveform is acquired through the Heisenberg transform, which can be seen as first operating $Nfft$ point IDFT for each symbol $\mathbf{X}_i$ and concatenating together into a long symbol $\mathbf{x} \in \mathbb{C}^{NfftN\times 1}$, given by

$$\mathbf{x} = \left[\mathbf{x}_1^T, \mathbf{x}_2^T, \ldots, \mathbf{x}_N^T\right]^T, \tag{15}$$

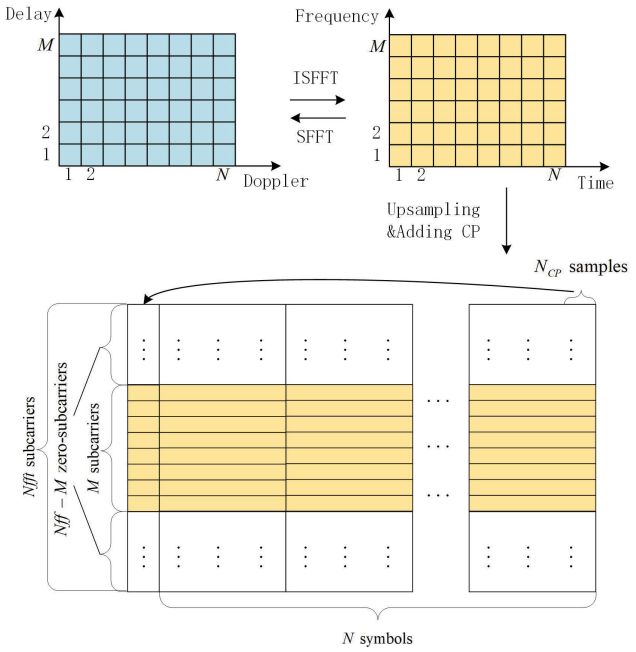

FIGURE 4. OTFS modulation and its time frequency structure in existing studies.

with

$$\mathbf{x}_i = \mathbf{G}_{tx}\mathbf{F}_{M}^{H}\mathbf{X}_i, \tag{16}$$

where $\mathbf{G}_{tx}$ is the pulse shaping matrix. For rectangular pulse shaping with upsampling, $\mathbf{G}_{tx}$ is equivalent to the zero padding matrix $\mathbf{Z}$. One CP is added before $\mathbf{x}$. This OTFS symbol structure has been widely adopted in existing studies. However, direct utilization of this structure may fail to coexist with NR protocol due to its modified 2D frame structure and transmission rate, which brings more challenges in flexible frame and packet length design, phase compensation, and windowing, etc. As a result, many existing parameters and procedures in NR physical layer and higher layers need to be redesigned.

C. PROPOSED BS-OFDM WITH PRE-PROCESSING

In Section III-B, the compatibility issue between NR protocol and OTFS was raised. One potential solution is to perform re-segmentation within a single OFDM symbol. Therefore, a scalable waveform scheme, named block scalable OFDM (BS-OFDM), is proposed for NR-enabled NTN. The proposed BS-OFDM is compatible to pre-processing schemes to generate BS-DFT-s-OFDM and BS-OTFS waveforms. A BS waveform framework is further developed, as shown in Fig.6, where the transmitter consists of constellation mapping, block mapping, pre-processing, zero padding, Heisenberg transform, CP insertion, and HPA, the receiver consists of CP removal, block equalization, Wigner transform, nonzero extraction, block demapping, and constellation demapping.

1) PROPOSED BS-OFDM

The time frequency structure of BS-OFDM is shown in Fig.5, where one OFDM symbol with data length M and SCS

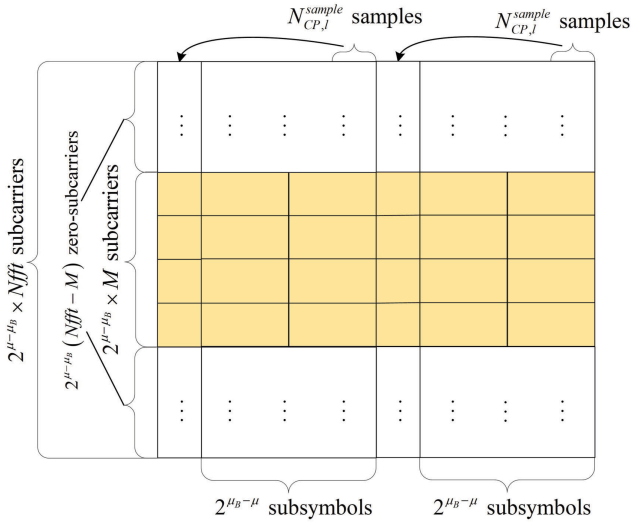

FIGURE 5. Time frequency structure of BS-OFDM.

configuration μ is re-segmented into M_B subcarriers and N_B sub-symbols, $N_B \geq 1$ and $M_B N_B = M$ are satisfied. The SCS of BS-OFDM is further defined as

$$\Delta f_B = 2^{\mu_B} \times 15\,[kHz]\,, \tag{17}$$

where μ_B is the SCS configuration of BS-OFDM. To preserve total bandwidth, the SCS of BS-OFDM follows

$$\begin{aligned} \Delta f_B &= M\,\Delta f\,/M_B \\ &= N_B \Delta f\,, \end{aligned} \tag{18}$$

substitute (11) and (17) into both sides of (18) and take the logarithm, we obtain

$$\mu_B = \mu + \log_2 N_B. \tag{19}$$

In order that Δf_B be a legal value specified in NR protocol, μ_B should be an integer, which means N_B should be chosen as a power of 2, as $N_B = 2^{\mu_B - \mu}$. The subcarrier number is thus modified as $M_B = M/N_B = M \times 2^{\mu-\mu_B}$. The number of IDFT points is also modified as $Nfft_B = Nfft \times 2^{\mu-\mu_B}$ so that the sample rate remains unchanged. Then, the time domain waveform can be obtained through zero padding and $Nfft_B \times N_B$ Heisenberg transform, presented as

$$\mathbf{x} = \left[\mathbf{x}_1^T, \mathbf{x}_2^T, \ldots, \mathbf{x}_{N_B}^T\right]^T, \tag{20}$$

with

$$\mathbf{x}_i = \mathbf{F}_{Nfft_B}^H \mathbf{Z}_B \mathbf{X}_i, \tag{21}$$

where $\mathbf{X}_i \in \mathbb{C}^{M_B \times 1}$ is the data in the i th sub-symbol and $\mathbf{Z}_B \in \mathbb{C}^{Nfft_B \times M_B}$ is a zero padding matrix.

One CP is added in front of the symbol block, the CP length is still relevant to μ and can be calculated by (12), which is the same as NR defined OFDM. Such structure holds the same time and frequency resource occupancy with an NR defined OFDM symbol of SCS configuration μ, thus guaranteeing the compatibility with the existing NR symbol structure without heavily modifying other NR operations such as phase compensation and windowing. As a result, most processing schemes in NR can still be used. In fact, the NR defined OFDM can be treated as a special case of our proposed BS-OFDM when $\mu_B = \mu$.

The proposed segmentation scheme is beneficial in several aspects. One important advantage of this segmentation is its increased flexibility in time and frequency diversity selection, since the time and frequency occupancy of one data symbol can be more flexibly configured for better diversity performance trade-offs in complex fading scenarios. Another advantage is that the PAPR can be reduced due to the reduction of subcarrier number, resulting in decreased total degradation and higher power efficiency in the presence of HPA nonlinearity. In addition, the modulation complexity is reduced compared to that of NR defined OFDM. The multiplication and addition times of $Nfft_B \times N_B$ Heisenberg transform operation are $\frac{1}{2}Nfft\left(\log_2 Nfft + \mu - \mu_B\right)$ and $N_B \times Nfft_B \log_2 Nfft_B = Nfft\left(\log_2 Nfft + \mu - \mu_B\right)$, respectively, when radix 2 fast Fourier transform (FFT) algorithm is utilized. It is observed that for fixed bandwidth and sample rate, the total computational complexity of BS-OFDM decreases as μ_B grows. Benefited from its compatibility with NR frame structure, our proposed BS-OFDM is also applicable in downlink or terrestrial scenarios.

At the receiver side, FDE is no longer applicable due to the inter sub-symbol interference in the 2D block structure when $N_B > 1$. As an alternative to FDE, message passing (MP) [20] and linear block equalization (BE) [26] can be implemented, resulting in increased complexity but better performance than FDE.

Taking the MMSE block equalizer as an example, the received signal after CP removal can be written as[1]

$$\mathbf{y}_{RCP} = \mathbf{H}_B \mathbf{x}_{RCP} + \mathbf{n}_{RCP}, \tag{22}$$

where $\mathbf{H}_B$ is a $Nfft_B N_B \times Nfft_B N_B$ matrix, given by

$$\mathbf{H}_B = \sum_{i=1}^{L} h_i \Pi^{l_i} \Delta^{(k_i)}, \tag{23}$$

where h_i, l_i, k_i are the channel path gain, normalized path delay, and normalized Doppler shift of the i th path, respectively, $\mathbf{\Pi}$ is a permutation matrix and $\mathbf{\Delta}^{(k_i)}$ is a diagonal matrix, given by

$$\mathbf{\Pi} = \begin{bmatrix} 0 & \cdots & 0 & 1 \\ 1 & \ddots & 0 & 0 \\ \vdots & \ddots & \ddots & \vdots \\ 0 & \cdots & 1 & 0 \end{bmatrix}_{Nfft_B N_B \times Nfft_B N_B}, \tag{24}$$

[1]Throughout this paper, MMSE BE is utilized in the simulation due to its wider application range and relatively lower complexity compared to MP. Note that this type of BE is also applicable for the baseline NR defined OFDM where $N_B = 1$.

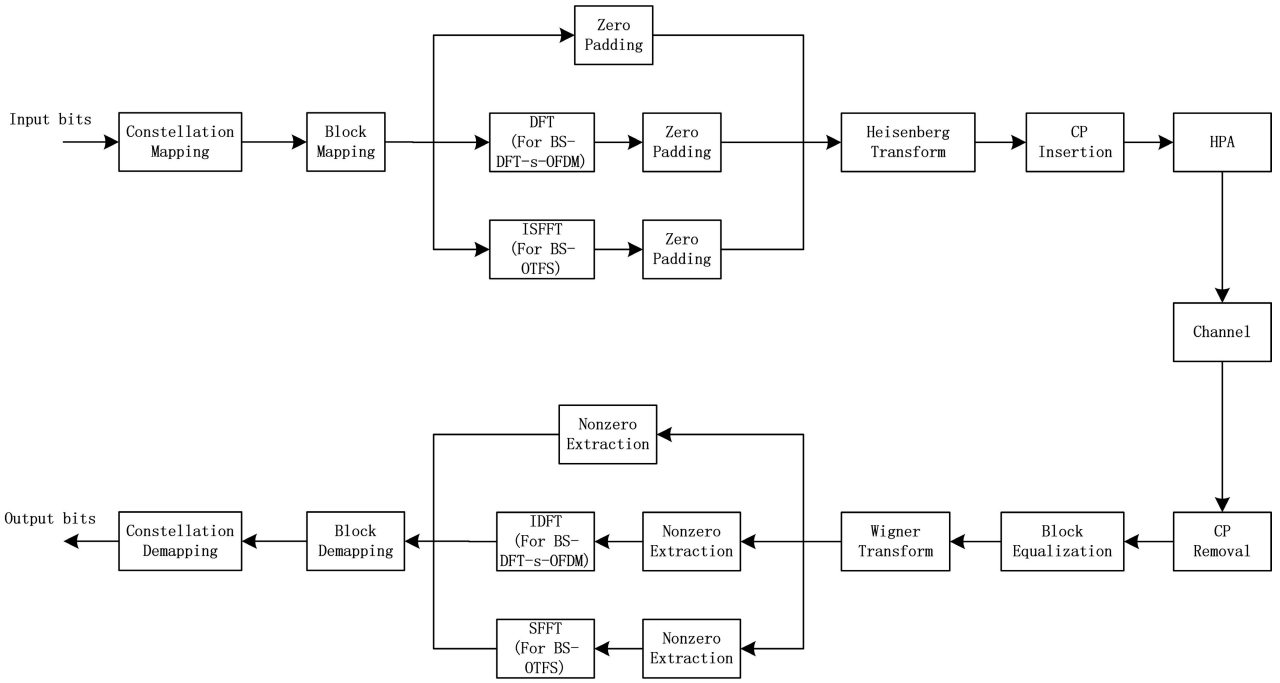

FIGURE 6. Transceiver framework for BS waveforms.

$$\mathbf{\Delta}^{(k_i)} = \begin{bmatrix} e^{\frac{j2\pi k_i(0)}{N_{fft_B} N_B}} & 0 & \cdots & 0 \\ 0 & e^{\frac{j2\pi k_i(1)}{N_{fft_B} N_B}} & \cdots & 0 \\ \vdots & \vdots & \ddots & \vdots \\ 0 & 0 & \cdots & e^{\frac{j2\pi k_i(N_{fft_B} N_B - 1)}{N_{fft_B} N_B}} \end{bmatrix}. \tag{25}$$

From (22), the time domain equalization can be expressed as

$$\mathbf{y}_{eq} = \mathbf{C}_B \mathbf{y}_{RCP}, \tag{26}$$

where $\mathbf{C}_B$ is the MMSE equalizer, given by

$$\mathbf{C}_B = \mathbf{H}_B{}^H / \left(\mathbf{H}_B{}^H \mathbf{H}_B + \sigma^2 \right), \tag{27}$$

$\mathbf{y}_{eq}$ is the concatenation of N_B sub-symbols, given by

$$\mathbf{y}_{eq} = \left[\mathbf{y}_{eq,1}^T, \mathbf{y}_{eq,2}^T, \ldots, \mathbf{y}_{eq,N_B}^T \right]^T, \tag{28}$$

The BER performance of MMSE BE and MMSE FDE for NR defined OFDM in S band and Ka band are plotted in Fig.7 and Fig.8, respectively, which consider both GEO and LEO NLOS linear channel. It can be observed that BE shows significant performance gain over FDE, especially in LEO scenarios where the BER of FDE are approximately 50%.

After equalization, the time domain signal $\mathbf{y}_{eq}$ is transformed into the TF domain block $\mathbf{Y}_{eq}$ through the Wigner transform, which is the inverse operation of the Heisenberg transform, given by

$$\mathbf{Y}_{eq} = \left[\mathbf{Y}_{eq,1}, \mathbf{Y}_{eq,2}, \ldots, \mathbf{Y}_{eq,N_B} \right], \tag{29}$$

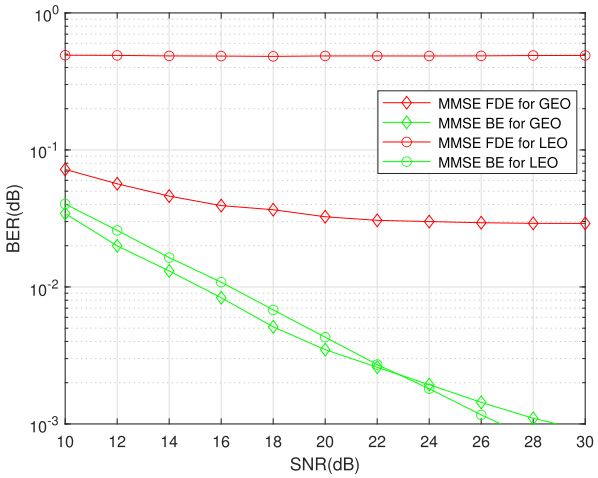

FIGURE 7. FDE versus BE in S band NLOS Linear channel.

with

$$\mathbf{Y}_{eq,i} = \mathbf{F}_{N_{fft_B}} \mathbf{y}_{eq,i}. \tag{30}$$

Finally, the symbol block $\mathbf{Y} \in \mathbb{C}^{M_B \times N_B}$ containing nonzero subcarriers is extracted from $\mathbf{Y}_{eq}$ through $\mathbf{Z}_B^T$, which is denoted by

$$\mathbf{Y} = \mathbf{Z}_B^T \mathbf{Y}_{eq}. \tag{31}$$

2) PRE-PROCESSING SCHEMES

To obtain better performance in nonlinear and fading channels, pre-processing schemes can be implemented before

TABLE 2. Computational complexity of different operations.

Processing step	Heisenberg/Wigner Transform (for all)	DFT spread/ IDFT despread (for BS-DFT-s-OFDM)	ISFFT/SFFT (for BS-OTFS)	Block Equalization (for all)
complexity	$\frac{3}{2}N_B Nfft_B \log_2 Nfft_B$	$\frac{3}{2}N_B M_B \log_2 M_B$	$\frac{3}{2}\left(N_B M_B \log_2 M_B + M_B N_B \log_2 N_B\right)$	$2Nfft^2 - Nfft$

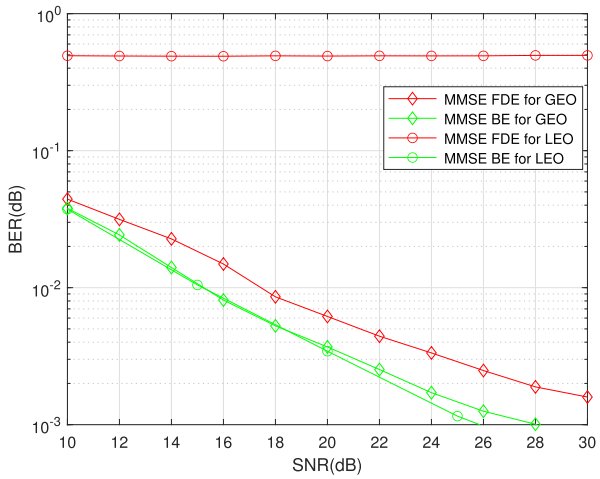

FIGURE 8. FDE versus BE in Ka band NLOS Linear channel.

BS-OFDM modulation to form BS-DFT-s-OFDM or BS-OTFS waveforms. To be noticed, these three types of waveforms can be realized through the same framework, as shown in Fig.6.

In BS-DFT-s-OFDM, M symbols are mapped to a block $\mathbf{X}_{spread} \in \mathbb{C}^{M_B \times N_B}$, note that when $M_B = M$ and $N_B = 1$, this representation reduces to NR defined DFT-s-OFDM.

BS-DFT-s-OFDM adds an M_B point DFT spread to $\mathbf{X}_{spread}$ before a BS-OFDM modulation (zero padding and the Heisenberg Transform), given by

$$\mathbf{X} = \mathbf{F}_{M_B}\mathbf{X}_{spread}. \tag{32}$$

As shown in Fig.6, the subsequent steps are the same as BS-OFDM, i.e., $\mathbf{X}$ is zero padded and transformed into the time domain waveform $\mathbf{x}$ through the Heisenberg transform, and then CP is added. After CP removal at the receiver, the signal $\mathbf{y}_{RCP}$ is block equalized into $\mathbf{y}_{eq}$ and transformed into the TF domain through Wigner transform, then the TF domain signal block $Y \in \mathbb{C}^{M_B \times N_B}$ is extracted.

An IDFT is implemented to obtain the time domain signal block $\mathbf{Y}_{spread}$, given by

$$\mathbf{Y}_{spread} = \mathbf{F}_{M_B}^H \mathbf{Y}. \tag{33}$$

BS-OTFS can also be treated as a scheme that adds pre-processing modules to a BS-OFDM symbol block. Firstly, at the transmitter, the symbols are mapped into a two-dimensional block $\mathbf{X}_{OTFS} \in \mathbb{C}^{M_B \times N_B}$ in the delay Doppler domain. The signal is then transformed into the TF domain through ISFFT as follows

$$\mathbf{X} = \mathbf{F}_{M_B}\mathbf{X}_{OTFS}\mathbf{F}_{N_B}^H. \tag{34}$$

The subsequent steps until the extraction of the TF domain signal block $\mathbf{Y}$ are also the same as BS-OFDM. Finally, before block demapping, a symplectic finite Fourier transform (SFFT) is implemented to obtain the DD domain signal block $\mathbf{Y}_{OTFS}$, given by

$$\mathbf{Y}_{OTFS} = \mathbf{F}_{M_B}^H \mathbf{Y}\mathbf{F}_{N_B}. \tag{35}$$

D. PERFORMANCE METRICS

In the proposed BS waveform framework, each combination of N_B and pre-processing scheme can be treated as an individual candidate waveform. In order to assess the effectiveness of various candidate waveforms under nonlinear NTN channels, performance metrics such as PAPR, total degradation, BER, and complexity are considered in performance comparison.

1) CCDF OF PAPR

The complementary cumulative distribution function (CCDF) of PAPR is an essential performance metric, which determines the vulnerability of the signal to nonlinear distortion.

Considering a time domain symbol block $\mathbf{z}$ with $Nfft$ samples, the PAPR is defined as

$$PAPR = \frac{\max\limits_{1 \le k \le Nfft} \left\{|\mathbf{z}(k)|^2\right\}}{P_{av}}, \tag{36}$$

where the average power P_{av} is given by

$$P_{av} = \frac{1}{Nfft}\sum_{k=1}^{Nfft} \mathbf{z}^*(k)\,\mathbf{z}(k). \tag{37}$$

For proposed candidate waveforms with upsampling and rectangular pulse shaping, the PAPR is not only relevant to specific M_B and N_B, but depends on pre-processing and constellation modulation schemes as well.

2) TOTAL DEGRADATION

Although the CCDF of PAPR is an important performance metric for waveforms, it is not directly relevant to the BER performance in the presence of nonlinear HPA. To this end, the total degradation (TD) [55] corresponding to the best operating output backoff (OBO) is provided, defined as

$$TD\,(dB) = OBO\,(dB) + SNR_{nl}\,(dB) - SNR_l\,(dB). \tag{38}$$

Instead of a function of input backoff (IBO), OBO also depends on the waveform type, modulation, and subcarrier number. SNR_l and SNR_{nl} are the required SNR for a target BER at 10^{-3} in AWGN channel under linear and nonlinear HPA, respectively. For QPSK modulation, we have $SNR_l =$

TABLE 3. Simulation parameters for different waveforms.

parameter \ deployment	Deployment-D1	Deployment-D2	Deployment-D3	Deployment-D4
Platform orbit and altitude	GEO at 35 786 km	GEO at 35 786 km	LEO at 600 km	LEO at 600 km
Carrier Frequency	Around 30 GHz for UL (Ka band)	Around 2 GHz for UL (S band)	Around 2 GHz for UL (S band)	Around 30 GHz for UL (Ka band)
Channel Bandwidth BW	12.96 MHz	360 kHz	360 kHz	12.96 MHz
UE type	VSAT	Handheld UE	Handheld UE	VSAT
Max Doppler shift in kHz	For plane @30 GHz: +/- 27.7 kHz	For plane @ 2 GHz: +/-1.851 kHz	@ 2 GHz : +/- 48 kHz	@30 GHz : +/- 720 kHz
Subcarrier spacing configuration μ_B	For NR defined OFDM and DFT-s-OFDM : 2 Otherwise: 3,4,5	For NR defined OFDM and DFT-s-OFDM : 0 Otherwise: 1,2,3	For NR defined OFDM and DFT-s-OFDM : 0 Otherwise: 1,2,3	For NR defined OFDM and DFT-s-OFDM : 2 Otherwise: 3,4,5
Subcarrier spacing Δf in kHz	$2^{\mu_B} \times 15$	$2^{\mu_B} \times 15$	$2^{\mu_B} \times 15$	$2^{\mu_B} \times 15$
Number of consecutive OFDM symbols N_B	2^{μ_B-2}	2^{μ_B}	2^{μ_B}	2^{μ_B-2}
FFT length $Nfft_B$	$2^{2-\mu_B} \times 256$	$2^{-\mu_B} \times 128$	$2^{-\mu_B} \times 128$	$2^{2-\mu_B} \times 256$
Modulation	QPSK	QPSK	QPSK	QPSK
Channel fading model	For NLOS channel: NTN-TDL-B For LOS channel: NTN-TDL-C	For NLOS channel: NTN-TDL-B For LOS channel: NTN-TDL-C	For NLOS channel: NTN-TDL-B For LOS channel: NTN-TDL-C	For NLOS channel: NTN-TDL-B For LOS channel: NTN-TDL-C

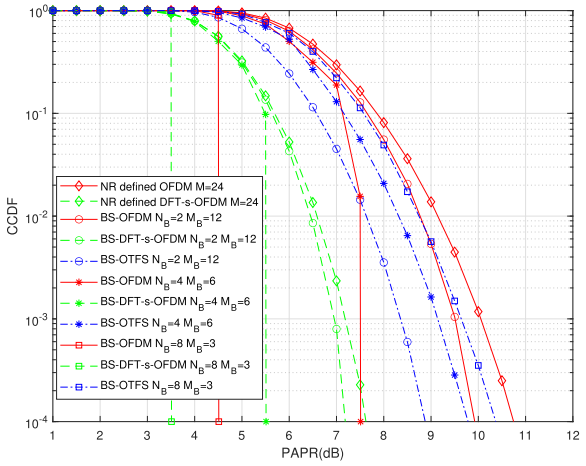

FIGURE 9. CCDF of PAPR in S band.

9.8dB for all orthogonal waveforms [9]. SNR_{nl} relevant to a particular OBO should be obtained individually for each case through simulation.

3) BER UNDER NONLINEAR NTN CHANNEL

The BER is a key metric measuring transmission reliability, which quantifies the rate at which errors occur in the transmission of binary data over a communication system. For each NTN scenario with a specific OBO value, the BER of different waveforms should be simulated individually for further performance comparison. More details of simulations and comparisons will be given in Section IV.

4) COMPUTATIONAL COMPLEXITY

Complexity is another important metric for NTN uplink, which is directly relative to hardware cost, power consumption, processing speed, etc. In this paper, we characterize the complexity by the total complex multiplication and addition times. For one symbol block, the computational complexity of each processing step is listed in Table 2.

From Table 2, it is noted that the complexity of BE dominates in the receiver processing, which results in almost the same receiver complexity for all candidate waveforms. The other receiver processings are all inverse operations of transmitter processings, therefore only transmitter complexity is performed in our comparison.

IV. PERFORMANCE COMPARISON AND DISCUSSIONS

In this section, the simulation concerning the performance of BS-OFDM, BS-DFT-s-OFDM and BS-OTFS, with different μ_B is provided. Furthermore, the simulation parameters are selected based on the NR numerology and NTN uplink scenarios with different UE type.[2] For fairness, the different waveforms are compared under the same bandwidth and time duration by fixing the $M_B N_B$ and adjustable subcarrier spacing configuration μ_B. We adopt NTN-TDL-B for non-line-of-sight (NLOS) cases and NTN-TDL-C for line-of-sight (LOS) cases, where a delay spread (DS) of 300ns is also considered [48]. For GEO satellite, the Doppler shift is mainly determined by UE mobility, where we assume that the maximum velocity of the UE is 1000km/h,[3] thus making maximum Doppler shifts to be 1.851kHz and 27.7kHz for S band (2GHz) and Ka band (30GHz) in the uplink, respectively. For LEO satellite, the Doppler shift caused by satellite motion becomes predominant, the maximum Doppler shifts in the uplink are 48kHz and 720kHz for S band and Ka band, respectively, at an orbit altitude of 600km [2]. All the relevant simulation parameters are listed in Table 3.

[2]The uplink bandwidth is $360kHz$ ($15kHz \times 24$) for S band handheld terminal, and $12.96MHz$ ($60kHz \times 216$) for Ka band VSAT [1].

[3]The speed of aircraft can be up to 1000km/h, which can be regarded as the extreme case of our considered system.

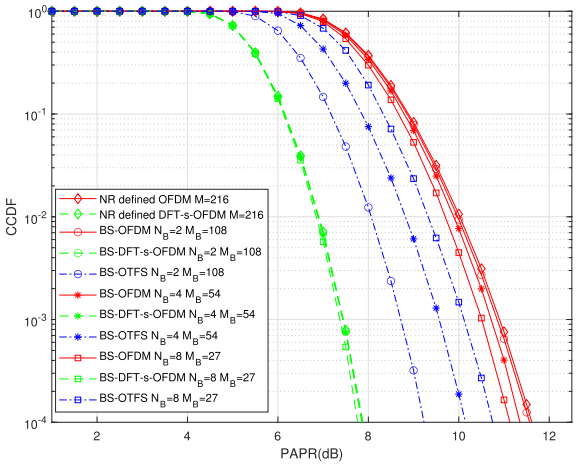

FIGURE 10. CCDF of PAPR in Ka band.

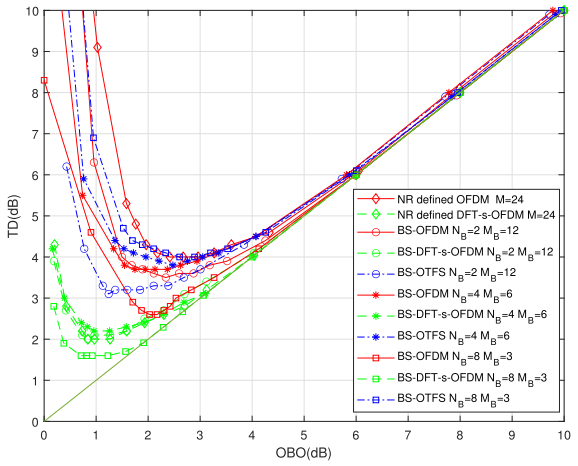

FIGURE 11. TD vs OBO in S band.

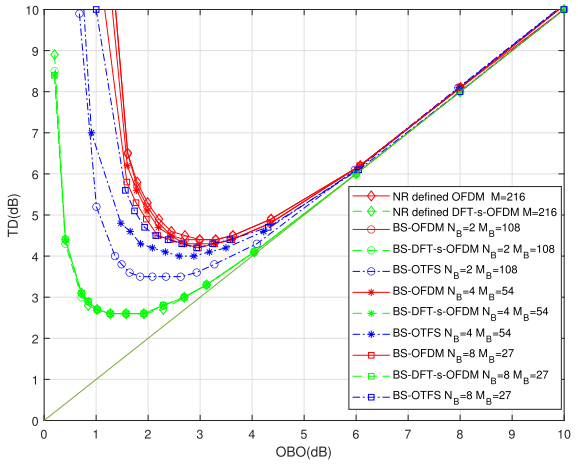

FIGURE 12. TD vs OBO in Ka band.

A. PAPR COMPARISON

Fig.9 shows the CCDF of PAPR in S band scenarios where $M_B N_B = 24$. The NR defined OFDM when $N_B = 1$ has the highest PAPR, BS-OFDM with other N_B values have relatively lower PAPR. Particularly, for small M_B values, the maximum PAPR of OFDM symbol is upper bounded by

$$PAPR_{\max,OFDM} = M_B \frac{\max_{c\in\mathbb{A}} |c|^2}{E\left\{|\mathbf{x}|^2\right\}}, \tag{39}$$

where $\mathbb{A}$ is the constellation set, the upper bound is approximately 7.5dB for $M_B = 6$ and 4.5dB for $M_B = 3$. BS-DFT-s-OFDM waveforms have the lowest PAPR for all M_B and N_B values, the PAPR is also bounded by about 5.5dB and 3.5dB for small subcarrier number $M_B = 6$ and $M_B = 3$, respectively. The PAPR of BS-OTFS is lower than BS-OFDM when $N_B = 2$, while higher than BS-OFDM for larger N_B, in fact the PAPR of BS-OTFS grows with N_B but not M_B, as demonstrated in [44].

Fig.10 shows the CCDF of PAPR in Ka band scenarios where $M_B N_B = 216$. It can be observed that NR defined OFDM has the highest PAPR, BS-OFDM with other N_B values have slightly better PAPR performance. BS-DFT-s-OFDM waveforms hold low PAPR characteristics, for different M_B values the CCDF are close. The PAPR of BS-OTFS waveforms are close to those in S band scenarios.

TABLE 4. Optimum OBO and corresponding minimum TD.

Waveband	S band		Ka band	
Optimum parameters	OBO(dB)	TD(dB)	OBO(dB)	TD(dB)
OFDM $N = 1$ (NR defined)	2.4	4.0	3.0	4.4
DFT-s-OFDM $N = 1$ (NR defined)	0,8	2.0	1.3	2.6
BS-OFDM $N_B = 2$	2.3	3.5	2.7	4.4
BS-DFT-s-OFDM $N_B = 2$	0.8	2.0	1.3	2.6
BS-OTFS $N_B = 2$	1.2	3.1	1.8	3.5
BS-OFDM $N_B = 4$	1.7	3.7	2.7	4.3
BS-DFT-s-OFDM $N_B = 4$	1.0	2.3	1.3	2.6
BS-OTFS $N_B = 4$	2.5	3.8	2.6	4.0
BS-OFDM $N_B = 8$	2.0	2.6	3.0	4.2
BS-DFT-s-OFDM $N_B = 8$	0.7	1.6	1.3	2.6
BS-OTFS $N_B = 8$	2.6	4.0	2.9	4.2

B. TOTAL DEGRADATION COMPARISON

The TD versus OBO curves of different waveforms are shown in Fig. 11 and Fig.12. For each waveform, the optimum OBO operating point for the HPA is the one that presents the lowest TD. For example, the minimum TD of NR defined OFDM are about 4.0 dB for S band and 4.4 dB for Ka band and the corresponding optimum OBO are 2.0 dB and 3.0 dB, respectively. The optimum OBO and corresponding minimum TD are summarized in Table 4. The proposed BS-DFT-s-OFDM waveforms show lower minimum TD, which

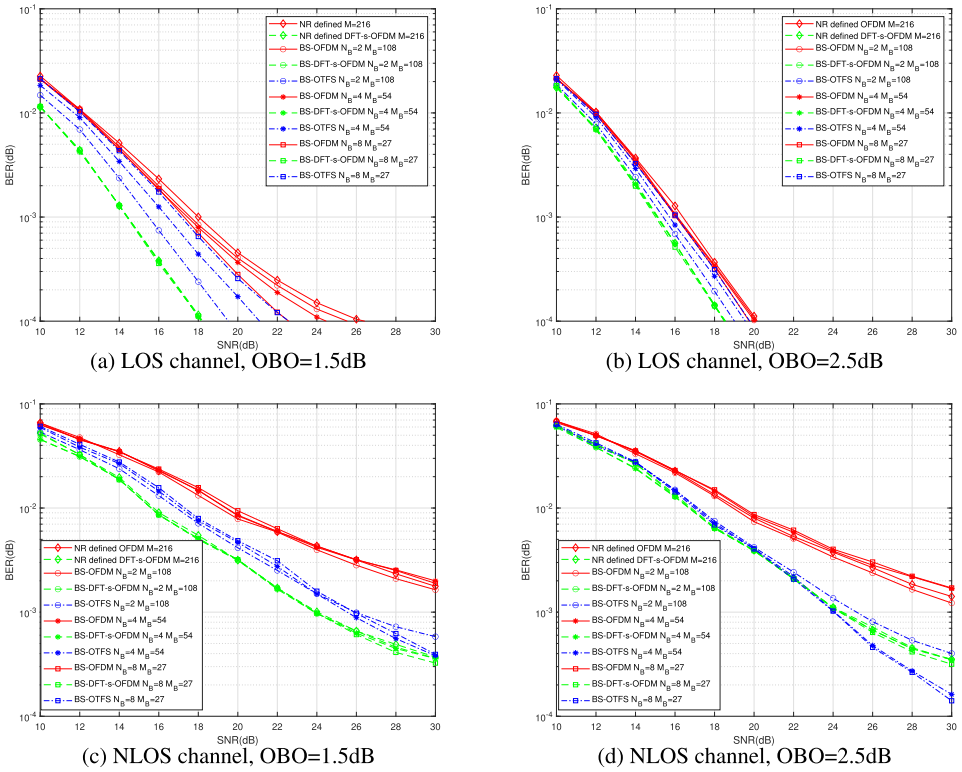

(a) LOS channel, OBO=1.5dB (b) LOS channel, OBO=2.5dB

(c) NLOS channel, OBO=1.5dB (d) NLOS channel, OBO=2.5dB

FIGURE 13. Waveform BER comparison in Ka band GEO scenarios.

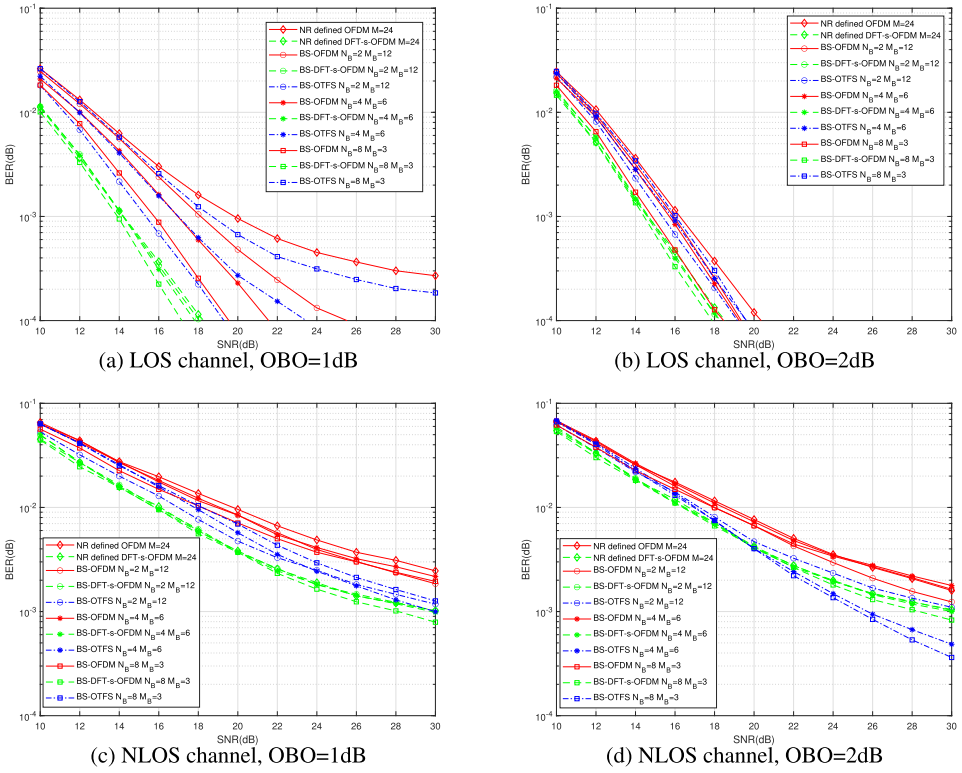

(a) LOS channel, OBO=1dB (b) LOS channel, OBO=2dB

(c) NLOS channel, OBO=1dB (d) NLOS channel, OBO=2dB

FIGURE 14. BER performance comparison in S band GEO scenarios.

occurs at around 1 dB and 1.5 dB OBO for S band and Ka band, respectively. For BS-OFDM and BS-OTFS waveforms, the minimum TD occurs at around 2 dB and 2.5 dB OBO for S band and Ka band, respectively.

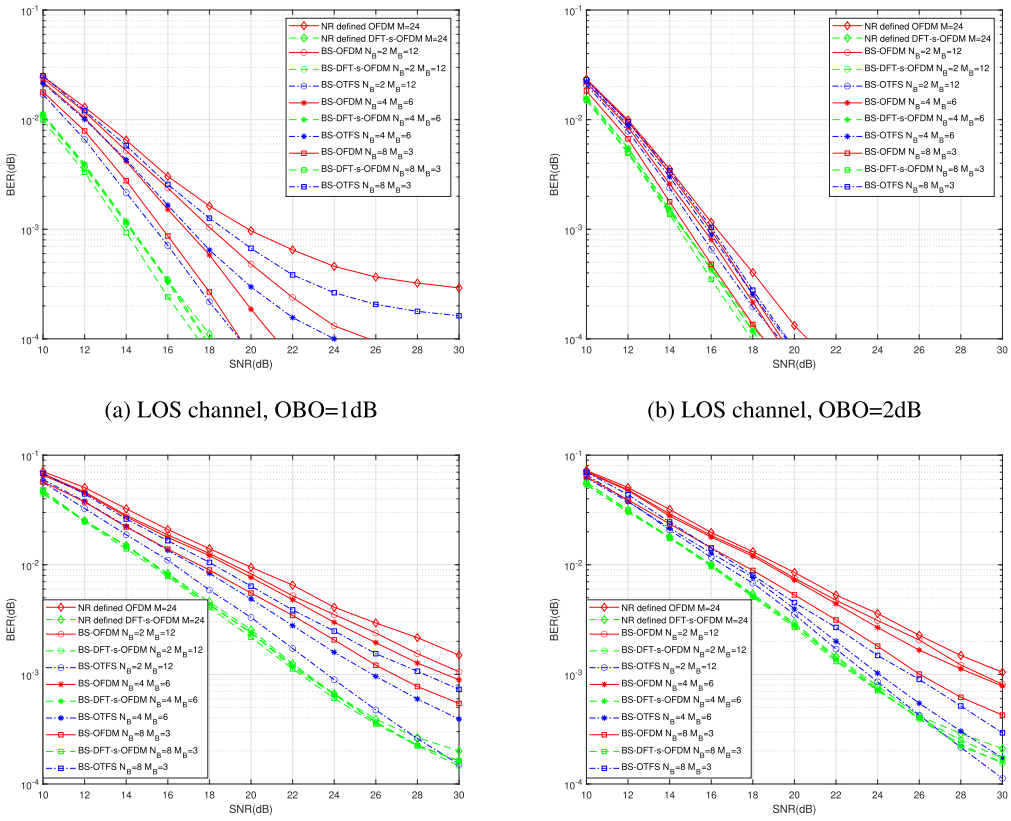

(a) LOS channel, OBO=1dB

(b) LOS channel, OBO=2dB

(c) NLOS channel, OBO=1dB

(d) NLOS channel, OBO=2dB

FIGURE 15. BER performance comparison in S band LEO scenarios.

C. BER PERFORMANCE COMPARISON

In this section, the BER performances of the waveforms under four NTN Deployment scenarios in Table 3 are presented. We assume that channel path gains and Dopplers are perfectly known at the receiver, all the transmitted data are uncoded, and the same MMSE BE is used for all the waveforms. A nonlinear HPA with predistortion is also considered. The backoff values are selected splitting the difference between the optimal OBO of each waveform, for S band scenarios OBO=1dB and OBO=2dB are used as low and high OBO, respectively, while for Ka band scenarios OBO=1.5dB and OBO=2.5dB are used.

1) DEPLOYMENT-D1 (Ka BAND GEO)

From Fig.13(a) and Fig.13(b), it can be observed that for NTN LOS channels, BS-DFT-s-OFDM waveforms outperform other candidate waveforms. The BER of BS-OFDM waveforms are higher than pre-processing waveforms, where the NR defined OFDM waveform shows the worst performance. The BER of BS-OTFS falls between BS-DFT-s-OFDM and BS-OFDM, which deteriorates as the number of sub-symbols increases. These results are attributed to the fact that the delay characteristics of the NTN LOS channels closely resemble a flat fading channel, where deep fading does not occur, and therefore TD plays an overwhelmingly dominant role in the nonlinear BER performance. As OBO increases, the nonlinear effects of HPA also weaken, for different waveforms there is no significant performance gap, similar to the linear flat fading channel.

From Fig.13(c), it is noted that with low OBO in the current scenario for NTN NLOS channels, the BS-DFT-s-OFDM waveforms still maintain the best performance, the performance ranking among different sub-symbol numbers in BS-OTFS changes, mainly due to the strong time frequency selectivity in NTN NLOS channels. From Fig.13(d), it is observed that as OBO increases, the time frequency diversity advantage of BS-OTFS gradually becomes dominant in terms of BER, counteracting the relative disadvantage compared to BS-DFT-s-OFDM in TD. Specifically, BS-OTFS with $N_B = 8$ exhibits optimal BER performance.

2) DEPLOYMENT-D2 (S BAND GEO)

From Fig.14(a) and Fig.14(b), it can be observed that the BER under the NTN LOS channel is still influenced by TD to a greater extent. When OBO increases from 1dB to 2dB, the performance gap between different waveforms decreases. It is noted that the BER performance of BS-OFDM with $N_B = 8$ is better than BS-OTFS with $N_B = 2$, which is contrary to the result of 1dB OBO. This is due to the difference in total degradation change of the two waveforms with the variation of OBO, as shown in Fig.11.

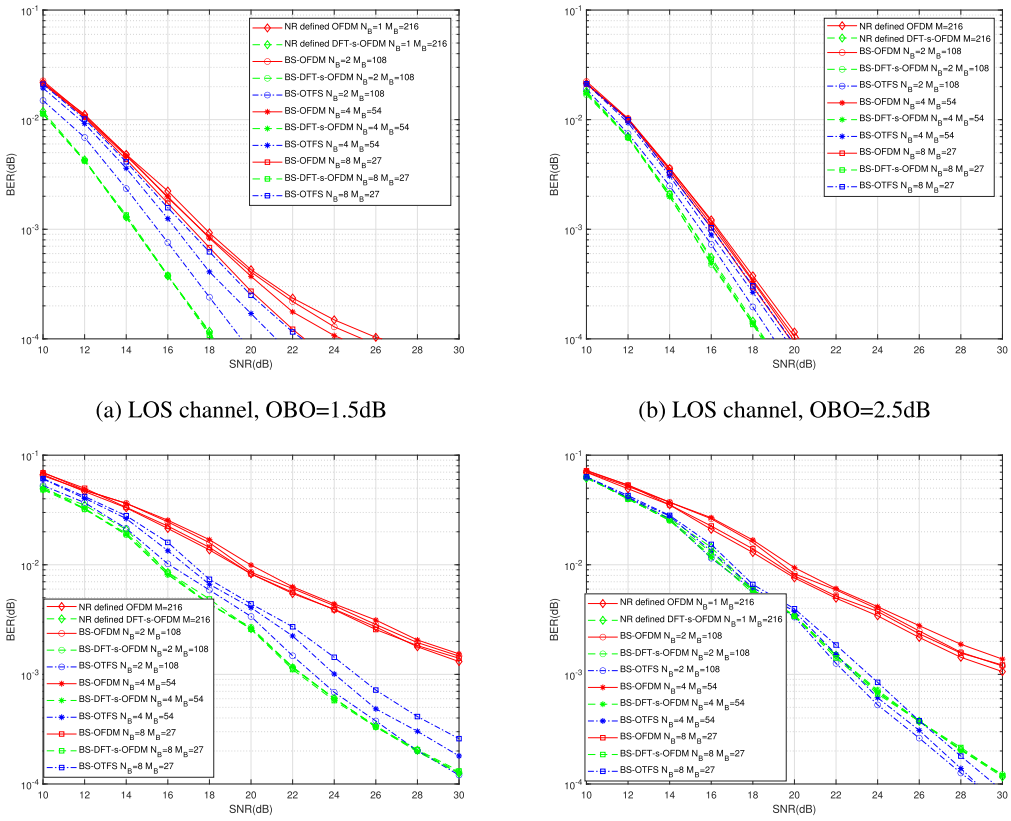

(a) LOS channel, OBO=1.5dB

(b) LOS channel, OBO=2.5dB

(c) NLOS channel, OBO=1.5dB

(d) NLOS channel, OBO=2.5dB

FIGURE 16. BER performance comparison in Ka band LEO scenarios.

From Fig.14(c) and Fig.14(d), similar conclusions as in the D1 scenario can be drawn. Due to the significant increase in the probability of deep fading in the NTN NLOS channel, the anti-fading performance of BS-OTFS is demonstrated. Under the condition of OBO=2dB, the anti-fading performance becomes dominant, and BS-OTFS with $N_B = 8$ achieves the optimal performance.

3) DEPLOYMENT-D3 (S BAND LEO)

As shown in Fig.15(a) and Fig.15(b), for the NTN LOS channel, the BER of each waveform exhibits similar results as the D2 scenario. The results demonstrate that the Doppler shift due to satellite mobility in the NTN LOS channel has a negligible impact on the occurrence of deep fading. After compensating the Doppler shift through block equalization, the signal can be regarded to experience flat fading.

From Fig.15(c) and Fig.15(d), it can be observed that the BER results are affected by both nonlinearity and deep channel fading. When OBO=1dB, the performances of BS-DFT-s-OFDM waveforms are superior. When OBO=2dB, BS-DFT-s-OFDM still outperform other waveforms at low SNR, and are not surpassed by BS-OTFS with $N_B = 2$ until SNR reaches 28dB, this is due to the large ratio of Doppler shift to the system bandwidth, which leads to significant channel variations over several BS-DFT-s-OFDM symbol periods in the time domain. As a result, the probability that continuous multiple symbols experiencing deep fading decreases, and the advantage in the time domain diversity of BS-OTFS over BS-DFT-s-OFDM is less significant.

4) DEPLOYMENT-D4 (Ka BAND LEO)

As shown in Fig.16(a) and Fig.16(b), for the NTN LOS channel, the BER of different waveforms exhibit similar results to the D1 scenario, for the same reasons as described in the previous scenario.

For Ka band LEO satellite with NLOS channel, the probability of deep fading is higher than that in S band scenario due to the increased overall bandwidth. Therefore, the impact of deep fading is more significant than in S band scenario. As shown in Fig.16(c), BS-DFT-s-OFDM waveforms have the lowest BER, since the impact of nonlinearity is still dominant when OBO=1.5dB. From Fig.16(d), it can be observed that BS-OTFS with $N_B = 2$ achieve the lowest BER when OBO=2.5dB. For BS-OTFS, higher N_B results in better resistance to deep fading, however it also results in higher total degradation due to the increased PAPR. This shows a trade-off between total degradation and resistance to deep fading. Specifically, in the current scenario,

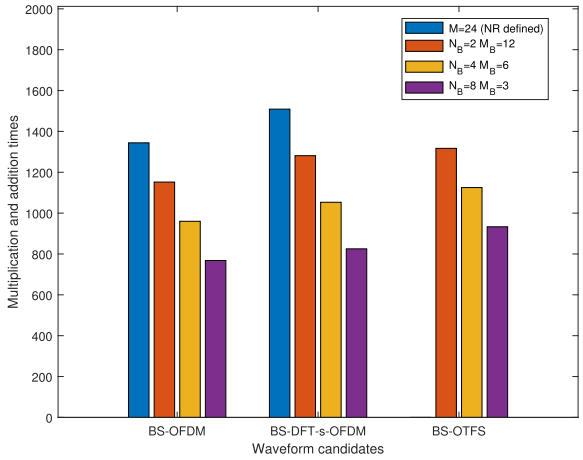

FIGURE 17. S band transmitter processing complexity.

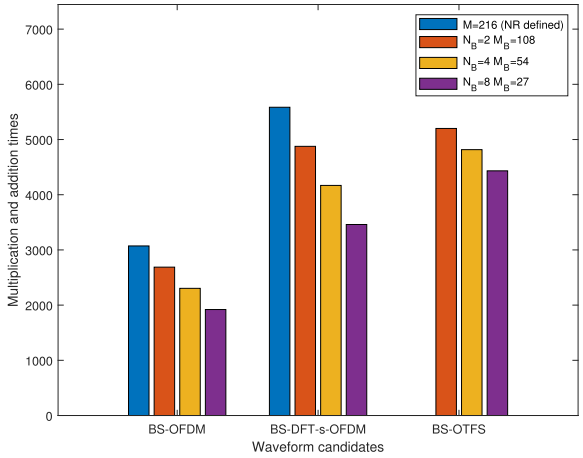

FIGURE 18. Ka band transmitter processing complexity.

BS-OTFS with $N_B = 2$ realizes a better trade-off than other candidate waveforms.

D. COMPUTATIONAL COMPLEXITY COMPARISON

Fig.17 shows the transmitter complexity for S band, it is observed that NR defined OFDM and DFT-s-OFDM have higher complexity than the proposed block scalable waveforms, since the complexity of the Heisenberg transform decreases as μ_B grows. For different pre-processing schemes with same μ_B, the complexities are close since the complexity of DFT spread and ISFFT are much lower than the Heisenberg transform when $M_B \ll Nfft_B$.

Fig.18 shows the transmitter complexity for Ka band. BS-OFDM waveforms have relatively lower complexity than pre-processing waveforms. Different from S band, M_B and $Nfft_B$ are close, the complexities increase more significantly when ISFFT and DFT spread are added. The NR defined DFT-s-OFDM still holds the highest complexity due to its relatively higher DFT spread and IDFT points than other waveforms.

E. DISCUSSIONS

In this section, the simulation results are summarized and compared. Considering both error performance and complexity, the recommended waveforms for different scenarios are provided.

In S band scenarios, BS-DFT-s-OFDM waveforms show significant advantages in BER over other waveforms under the LOS channel and the NLOS channel with low OBO due to low PAPR characteristics. Among them, BS-DFT-s-OFDM with $N_B = 8$ has relatively lowest processing complexity. For the NLOS channel with high OBO, BS-OTFS with $N_B = 8$ is recommended for the GEO scenario due to its better BER performance and negligible complexity increment over BS-DFT-s-OFDM. For LEO scenarios, BS-DFT-s-OFDM with $N_B = 8$ is still recommended, since the optimal performance of BS-OTFS with $N_B = 2$ only occurs at a very low BER level, as well a cost of about 50% complexity increase over BS-DFT-s-OFDM with $N_B = 8$.

In Ka band scenarios, although BS-OFDM waveforms without pre-processing have relatively lower complexity than pre-processing block waveforms, significant loss in BER performances are observed, especially for the NLOS channel. For LOS and low OBO NLOS cases, BS-DFT-s-OFDM with $N_B = 8$ is recommended for its advantage in BER and relatively less increased complexity, just as in the S band. For NLOS channel with high OBO, BS-OTFS with $N_B = 8$ and $N_B = 2$ are recommended for GEO and LEO satellite, respectively, due to the relatively better trade-offs between TD, time frequency diversity, and complexity.

V. CONCLUSION

In this paper, a BS-OFDM based waveform framework is proposed to combat the Doppler effect and nonlinearity in the NTN uplink channel, which has the same time and frequency occupancy with existing NR waveforms, and is therefore compatible with NR protocol. Furthermore, DFT spread and ISFFT pre-processing can be implemented for performance improvement. A comparative study of the proposed and existing waveforms over different NTN deployment scenarios is conducted, considering multiple metrics including PAPR, TD, BER, and complexity. The promising waveform for each particular NTN deployment scenario is determined. In a nutshell, this paper recommends BS-DFT-s-OFDM with 8 sub-symbols for the LOS channel and the NLOS channel with low OBO in all NTN deployment scenarios, and also for the NLOS channel with high OBO in S band LEO scenarios. BS-OTFS with 8 sub-symbols is recommended for the NLOS channel with high OBO in Ka and S band GEO scenarios. BS-OTFS with 2 sub-symbols is recommended for the NLOS channel with high OBO in Ka band GEO scenarios.

VI. FUTURE WORKS

This paper assumes a single user and single antenna case with perfect synchronization and known channel information at the receiver, which can be extended to more complicated or non-ideal cases. Our future works will focus on multiuser asynchronous receiver design, phase noise elimination, extension to massive MIMO systems, reference signal design,

and channel estimation for BS-OFDM based waveforms in NTN scenarios. Moreover, other improvements in BS-OFDM based waveforms like pre-processing scheme optimization, PAPR and OOBE reduction can also be considered in the future.

REFERENCES

[1] *Solutions for NR to Support Non-Terrestrial Networks (NTN)*, document TR 38.821, 3GPP, 2021.

[2] *Study New Radio (NR) to Support Non-Terrestrial Networks*, document TR 38.811, 3GPP, 2019.

[3] M. Hosseinian, J. P. Choi, S.-H. Chang, and J. Lee, "Review of 5G NTN standards development and technical challenges for satellite integration with the 5G network," *IEEE Aerosp. Electron. Syst. Mag.*, vol. 36, no. 8, pp. 22–31, Aug. 2021.

[4] W. Yuan, S. Li, Z. Wei, Y. Cui, J. Jiang, H. Zhang, and P. Fan, "New delay Doppler communication paradigm in 6G era: A survey of orthogonal time frequency space (OTFS)," *China Commun.*, vol. 20, no. 6, pp. 1–25, Jun. 2023.

[5] I. Ali, N. Al-Dhahir, and J. E. Hershey, "Doppler characterization for LEO satellites," *IEEE Trans. Commun.*, vol. 46, no. 3, pp. 309–313, Mar. 1998.

[6] A. Guidotti, A. Vanelli-Coralli, M. Conti, S. Andrenacci, S. Chatzinotas, N. Maturo, B. Evans, A. Awoseyila, A. Ugolini, T. Foggi, L. Gaudio, N. Alagha, and S. Cioni, "Architectures and key technical challenges for 5G systems incorporating satellites," *IEEE Trans. Veh. Technol.*, vol. 68, no. 3, pp. 2624–2639, Mar. 2019.

[7] O. Kodheli, S. Andrenacci, N. Maturo, S. Chatzinotas, and F. Zimmer, "An uplink UE group-based scheduling technique for 5G mMTC systems over LEO satellite," *IEEE Access*, vol. 7, pp. 67413–67427, 2019.

[8] M. Alsabah, M. A. Naser, B. M. Mahmmod, S. H. Abdulhussain, M. R. Eissa, A. Al-Baidhani, N. K. Noordin, S. M. Sait, K. A. Al-Utaibi, and F. Hashim, "6G wireless communications networks: A comprehensive survey," *IEEE Access*, vol. 9, pp. 148191–148243, 2021.

[9] *Satellite Earth Stations and Systems (SES), SC-FDMA Based Radio Wave-Form Technology for Ku/Ka Band Satellite Service*, document TR 103 297, ETSI, 2017.

[10] V. Dalakas, P. T. Mathiopoulos, F. Di Cecca, and G. Gallinaro, "A comparative study between SC-FDMA and OFDMA schemes for satellite uplinks," *IEEE Trans. Broadcast.*, vol. 58, no. 3, pp. 370–378, Sep. 2012.

[11] X. Liu, M. Liang, Y. Morton, P. Closas, T. Zhang, and Z. Hong, "Performance evaluation of MSK and OFDM modulations for future GNSS signals," *GPS Solutions*, vol. 18, no. 2, pp. 163–175, Apr. 2014.

[12] N. Cassiau, L. Maret, J.-B. Doré, V. Savin, and D. Kténas, "Assessment of 5G NR physical layer for future satellite networks," in *Proc. IEEE Global Conf. Signal Inf. Process.*, Nov. 2018, pp. 1020–1024.

[13] A. Jayaprakash, H. Chen, P. Xiao, B. G. Evans, Y. Zhang, J. Y. Li, and A. B. Awoseyila, "Analysis of candidate waveforms for integrated satellite-terrestrial 5G systems," in *Proc. IEEE 2nd 5G World Forum (5GWF)*, Dresden, Germany, Sep. 2019, pp. 636–641.

[14] A. Jayaprakash, B. G. Evans, P. Xiao, A. B. Awoseyila, and Y. Zhang, "New radio numerology and waveform evaluation for satellite integration into 5G terrestrial network," in *Proc. IEEE Int. Conf. Commun. (ICC)*, Dublin, Ireland, Jun. 2020, pp. 1–7.

[15] G. George, S. Roy, S. Raghunandan, C. Rohde, and T. Heyn, "5G new radio in nonlinear satellite downlink: A physical layer comparison with DVB-S2X," in *Proc. IEEE 4th 5G World Forum (5GWF)*, Montreal, QC, Canada, Oct. 2021, pp. 499–504.

[16] B. F. Beidas and R. I. Seshadri, "OFDM-like signaling for broadband satellite applications: Analysis and advanced compensation," *IEEE Trans. Commun.*, vol. 65, no. 10, pp. 4433–4445, Oct. 2017.

[17] Y. Li, X. Gu, L. Dan, R. He, X. Mao, and Y. Xiao, "Improved OFDM waveform for radio link in non-terrestrial network," in *Proc. Int. Symp. Netw., Comput. Commun. (ISNCC)*, Montreal, QC, Canada, Oct. 2020, pp. 1–6.

[18] L. Deng, Y. Yang, J. Ma, Y. Feng, L. Ye, and H. Li, "OFDM-BOC: A broadband multicarrier navigation modulation-based BOC for future GNSS," *IEEE Trans. Veh. Technol.*, early access, Oct. 2023, doi: 10.1109/TVT.2023.3328252.

[19] R. Hadani, S. Rakib, M. Tsatsanis, A. Monk, A. J. Goldsmith, A. F. Molisch, and R. Calderbank, "Orthogonal time frequency space modulation," in *Proc. IEEE Wireless Commun. Netw. Conf. (WCNC)*, San Francisco, CA, USA, Mar. 2017, pp. 1–6.

[20] P. Raviteja, K. T. Phan, Y. Hong, and E. Viterbo, "Interference cancellation and iterative detection for orthogonal time frequency space modulation," *IEEE Trans. Wireless Commun.*, vol. 17, no. 10, pp. 6501–6515, Oct. 2018.

[21] Y. Liang, L. Li, P. Fan, and Y. Guan, "Doppler resilient orthogonal time-frequency space (OTFS) systems based on index modulation," in *Proc. IEEE 91st Veh. Technol. Conf.*, May 2020, pp. 1–5.

[22] H. Zhao, D. He, Z. Kang, and H. Wang, "Orthogonal time frequency space (OTFS) with dual-mode index modulation," *IEEE Wireless Commun. Lett.*, vol. 10, no. 5, pp. 991–995, May 2021.

[23] C. Zhang, D. Feng, M. Liu, and B. Bai, "Spatial modulation based MIMO-OTFS transmissions," in *Proc. IEEE/CIC Int. Conf. Commun. China*, Jul. 2021, pp. 427–432.

[24] X. Zou, S. Fan, H. Chen, Y. Xiao, C. Di, and J. Ji, "Orthogonal time frequency space with generalized spatial modulation," in *Proc. IEEE 95th Veh. Technol. Conf.*, Jun. 2022, pp. 1–5.

[25] Y. Chen, L. Zhao, Y. Jiang, W. Li, H. Gao, and C. Liu, "OTFS waveform based on 3-D signal constellation for time-variant channels," *IEEE Commun. Lett.*, vol. 27, no. 8, pp. 1999–2003, Aug. 2023.

[26] H. Zhang, X. Huang, and J. A. Zhang, "Comparison of OTFS diversity performance over slow and fast fading channels," in *Proc. IEEE/CIC Int. Conf. Commun. China (ICCC)*, Aug. 2019, pp. 828–833.

[27] W. Anwar, A. Krause, A. Kumar, N. Franchi, and G. P. Fettweis, "Performance analysis of various waveforms and coding schemes in V2X communication scenarios," in *Proc. IEEE Wireless Commun. Netw. Conf. (WCNC)*, May 2020, pp. 1–8.

[28] W. Anwar, A. Kumar, N. Franchi, and G. Fettweis, "Physical layer performance modeling of modern multicarrier modulation techniques," *IEEE Trans. Commun.*, vol. 70, no. 6, pp. 3725–3741, Jun. 2022.

[29] S. Tarboush, H. Sarieddeen, M.-S. Alouini, and T. Y. Al-Naffouri, "Single- versus multicarrier terahertz-band communications: A comparative study," *IEEE Open J. Commun. Soc.*, vol. 3, pp. 1466–1486, 2022.

[30] J. Hu, J. Shi, S. Ma, and Z. Li, "Secrecy analysis for orthogonal time frequency space scheme based uplink LEO satellite communication," *IEEE Wireless Commun. Lett.*, vol. 10, no. 8, pp. 1623–1627, Aug. 2021.

[31] J. Shi, J. Hu, Y. Yue, X. Xue, W. Liang, and Z. Li, "Outage probability for OTFS based downlink LEO satellite communication," *IEEE Trans. Veh. Technol.*, vol. 71, no. 3, pp. 3355–3360, Mar. 2022.

[32] J. Hu, Y. Jin, J. Shi, X. Liu, Z. Dai, and Z. Li, "Reliability analysis of stochastic geometry-based multi-UAV-aided LEO-SATCOM under OTFS," in *Proc. Int. Symp. Wireless Commun. Syst. (ISWCS)*, Hangzhou, China, Oct. 2022, pp. 1–6.

[33] S. K. Devarajalu and D. Jose, "Performance evaluation of OTFS under different channel conditions for LEO satellite downlink," in *Proc. 10th Int. Conf. Wireless Netw. Mobile Commun. (WINCOM)*, Oct. 2023, pp. 1–6.

[34] M. Caus, M. Shaat, A. I. Pérez-Neira, M. Schellmann, and H. Cao, "Reliability oriented OTFS-based LEO satellites joint transmission scheme," in *Proc. IEEE Globecom Workshops*, Rio de Janeiro, Brazil, Dec. 2022, pp. 1406–1412.

[35] C. Li, L. Zhu, C. Guo, T. Liu, and Z. Zhang, "Intelligent blind source separation technology based on OTFS modulation for LEO satellite communication," *China Commun.*, vol. 19, no. 7, pp. 89–99, Jul. 2022.

[36] C. Xu, L. Xiang, J. An, C. Dong, S. Sugiura, R. G. Maunder, L.-L. Yang, and L. Hanzo, "OTFS-aided RIS-assisted SAGIN systems outperform their OFDM counterparts in doubly selective high-Doppler scenarios," *IEEE Internet Things J.*, vol. 10, no. 1, pp. 682–703, Jan. 2023.

[37] X. Wang, W. Shen, C. Xing, J. An, and L. Hanzo, "Joint Bayesian channel estimation and data detection for OTFS systems in LEO satellite communications," *IEEE Trans. Commun.*, vol. 70, no. 7, pp. 4386–4399, Jul. 2022.

[38] B. Shen, Y. Wu, J. An, C. Xing, L. Zhao, and W. Zhang, "Random access with massive MIMO-OTFS in LEO satellite communications," *IEEE J. Sel. Areas Commun.*, vol. 40, no. 10, pp. 2865–2881, Oct. 2022.

[39] B. Shen, Y. Wu, W. Zhang, G. Y. Li, J. An, and C. Xing, "LEO satellite-enabled grant-free random access with MIMO-OTFS," in *Proc. IEEE Global Commun. Conf.*, Rio de Janeiro, Brazil, Dec. 2022, pp. 3308–3313.

[40] X. Zhou, K. Ying, Z. Gao, Y. Wu, Z. Xiao, S. Chatzinotas, J. Yuan, and B. Ottersten, "Active terminal identification, channel estimation, and signal detection for grant-free NOMA-OTFS in LEO satellite Internet-of-Things," *IEEE Trans. Wireless Commun.*, vol. 22, no. 4, pp. 2847–2866, Apr. 2023.

[41] C. Guo, X. Chen, J. Yu, and Z. Xu, "Design of joint device and data detection for massive grant-free random access in LEO satellite Internet of Things," *IEEE Internet Things J.*, vol. 10, no. 8, pp. 7090–7099, Apr. 2023.

[42] Y. Ma, G. Ma, N. Wang, Z. Zhong, J. Yuan, and B. Ai, "Enabling OTFS-TSMA for smart railways mMTC over LEO satellite: A differential Doppler shift perspective," *IEEE Internet Things J.*, vol. 10, no. 6, pp. 4799–4814, Mar. 2023.
[43] *NR Physical Channels and Modulation*, document TS 38.211, 3GPP, 2021.
[44] G. D. Surabhi, R. M. Augustine, and A. Chockalingam, "Peak-to-average power ratio of OTFS modulation," *IEEE Commun. Lett.*, vol. 23, no. 6, pp. 999–1002, Jun. 2019.
[45] P. Wei, Y. Xiao, W. Feng, N. Ge, and M. Xiao, "Charactering the peak-to-average power ratio of OTFS signals: A large system analysis," *IEEE Trans. Wireless Commun.*, vol. 21, no. 6, pp. 3705–3720, Jun. 2022.
[46] F. Rinaldi, H.-L. Maattanen, J. Torsner, S. Pizzi, S. Andreev, A. Iera, Y. Koucheryavy, and G. Araniti, "Non-terrestrial networks in 5G & beyond: A survey," *IEEE Access*, vol. 8, pp. 165178–165200, 2020.
[47] G. D. Surabhi, R. M. Augustine, and A. Chockalingam, "On the diversity of uncoded OTFS modulation in doubly-dispersive channels," *IEEE Trans. Wireless Commun.*, vol. 18, no. 6, pp. 3049–3063, Jun. 2019.
[48] *Study on Channel Model for Frequencies From 0.5 to 100 GHz*, document TS 38.901, 3GPP, 2019.
[49] M. O'Droma, S. Meza, and Y. Lei, "New modified saleh models for memoryless nonlinear power amplifier behavioural modelling," *IEEE Commun. Lett.*, vol. 13, no. 12, p. 1007, Dec. 2009.
[50] T. Jiang, C. Li, and C. Ni, "Effect of PAPR reduction on spectrum and energy efficiencies in OFDM systems with class—A HPA over AWGN channel," *IEEE Trans. Broadcast.*, vol. 59, no. 3, pp. 513–519, Sep. 2013.
[51] E. Olfat and M. Bengtsson, "Joint channel and clipping level estimation for OFDM in IoT-based networks," *IEEE Trans. Signal Process.*, vol. 65, no. 18, pp. 4902–4911, Sep. 2017.
[52] H. Sari, G. Karam, and I. Jeanclaude, "Transmission techniques for digital terrestrial TV broadcasting," *IEEE Commun. Mag.*, vol. 33, no. 2, pp. 100–109, Feb. 1995.
[53] G. Araniti, A. Iera, S. Pizzi, and F. Rinaldi, "Toward 6G non-terrestrial networks," *IEEE Netw.*, vol. 36, no. 1, pp. 113–120, Jan. 2022.
[54] D. He, Z. Zhang, H. Lin, Z. Wu, Y. Huang, and Z. Wang, "Performance comparison of single-carrier and multi-carrier waveforms over terahertz wireless channels," *Digit. Commun. Netw.*, early access, Jul. 2023, doi: 10.1016/j.dcan.2023.07.001.
[55] A. N. D'Andrea, V. Lottici, and R. Reggiannini, "RF power amplifier linearization through amplitude and phase predistortion," *IEEE Trans. Commun.*, vol. 44, no. 11, pp. 1477–1484, Nov. 1996.

YUFAN CHEN received the B.S. degree in information engineering from Beijing Institute of Technology (BIT), Beijing, China, in 2018, where he is currently pursuing the Ph.D. degree in information and communication systems. His current research interests include non-terrestrial networks, waveform design, and channel estimation.

HAN LIU received the M.S. degree in digital communication system from the University of Sussex, Brighton, U.K., in 2013, and the Ph.D. degree in information and electronics from Beijing Institute of Technology (BIT), Beijing, China, in 2018. She is currently a Postdoctoral Research Fellow with the School of Information and Electronics, BIT. Her research interests include signal processing, object detection, and physical layer security.

ZHIPING LU received the M.S. degree in computer science from the University of Chinese Academy of Sciences, in 2008. He is currently pursuing the Ph.D. degree in information and communication engineering with Beijing University of Posts and Telecommunications and the State Key Laboratory of Wireless Mobile Communications, China Academy of Telecommunications Technology (CATT). His research interests include wireless communications and artificial intelligence.

HUA WANG (Member, IEEE) received the Ph.D. degree from Beijing Institute of Technology (BIT), Beijing, China, in 1999. From February 2009 to January 2010, he was a Visiting Professor with the Department of Electrical Engineering, Arizona State University, USA. He is currently a Professor with the School of Information and Electronics, BIT. His research interests include communication theory and signal processing, wireless networking, and modem design and implementation for satellite communication.